THE ASTROPHYSICAL JOURNAL, 348:611–620, 1990 January 10

THE SOURCE CHARGE AND ISOTROPIC ABUNDANCES OF COSMIC RAYS WITH $Z = 9$–16: A STUDY USING NEW FRAGMENTATION CROSS SECTIONS

W. R. WEBBER,[1] A. SOUTOUL,[2] P. FERRANDO,[2] AND M. GUPTA[1]

Received 1989 March 29; accepted 1989 July 8

ABSTRACT

We have reexamined the cosmic-ray source charge and isotopic abundances for charges with $Z = 9$–16 using newly measured fragmentation cross sections in a standard Galactic propagation model. Several important differences are found as compared with earlier studies. The cosmic-ray data are now consistent with no excess of ^{29}Si and ^{30}Si in the source relative to the solar coronal abundances. The excess of ^{25}Mg and ^{26}Mg is now $\sim 1\ \sigma$ or less relative to solar coronal isotopic abundances, leaving ^{22}Ne as the only clearly established neutron rich isotopic excess in the cosmic-ray source. The measurements of the radioactive decay isotope ^{26}Al now are interpreted as possibly implying a smaller matter density than obtained from ^{10}Be measurements.

Better estimates of the source abundances of elements obtained using the new cross sections have permitted the conclusion that high first ionization potential (FIP) elements have a wide spread of compositional differences in the cosmic-ray source relative to solar coronal abundances whereas elements with a low FIP have a composition similar to the solar corona. Clearly distinguished compositional differences, not explained by solar FIP effects alone exist for ^{4}He, ^{12}C, ^{14}N, ^{20}Ne, ^{22}Ne, and ^{32}S, among the elements studied. These differences can be explained by a combination of an enhanced FIP effect in the cosmic-ray sources, plus a contribution from Wolf-Rayet type sources.

Subject headings: cosmic rays: abundances — stars: abundances

I. INTRODUCTION

Cosmic rays in the charge range $Z = 9$–16 have been extensively measured. High-precision charge abundance data have been available for several years from the *HEAO* C-2 experiment (Engelmann *et al.* 1983) and from IMP 8 at lower energies (Garcia Munoz and Simpson 1979). Isotopic abundance data for Ne, Mg, and Si also exist from several experiments (Wiedenbeck and Greiner 1981*a*, *b*; Mewaldt *et al.* 1980; Webber 1982, 1985). The principal goal of all these measurements has been to provide a basis for determining the charge and isotopic composition of these nuclei at the cosmic-ray source. In the case of the odd nuclei, Fl, Na, Al, and P, the source abundance is quite small and most of the observed abundance of these nuclei at Earth is due to the interstellar fragmentation of heavier cosmic-ray nuclei. This is also true for some of the heavier isotopes of Ne, Mg, and Si. The abundance of several of these isotopes has been determined to be significantly larger in the cosmic-ray source than in solar system material (see, for example Wiedenbeck 1984), and this seems to provide an indication for a possible different nucleosynthetic history for the cosmic rays.

Recently the New Hampshire (UNH) group has completed an extensive series of measurements of almost all the important fragmentation cross sections into these charges from heavier nuclei in hydrogen targets (see, e.g., Webber 1984, 1987). The utilization of these cross sections has already led to a significant increase in the cosmic-ray path length in Galactic hydrogen as determined from the B/C ratio. New and significantly different source abundances have also been determined for ^{13}C and ^{14}N using these new cross sections in conjunction with previously measured abundance ratios (Gupta and Webber 1989; Webber and Soutoul 1989). In this paper we examine the effect of these new cross sections on the source abundance determinations of charges and isotopes with Z mainly between 9 and 16.

II. CROSS SECTIONS USED AND THE INTERSTELLAR PROPAGATION PROGRAM

In Table 1 we list the newly measured cross sections for the production of most of the nuclei with $Z = 9$–16. Not shown are the cross sections for the production of ^{20}Ne, ^{24}Mg, ^{28}Si, and ^{32}S since these isotopes are dominated by their source contribution. The cross sections of all of the fragment nuclei listed in Table 1 have been measured by the UNH group in one form or another—either the direct isotopic cross section decayed, e.g., $^{27}\text{Al} \rightarrow {}^{23}\text{Na}$; or the charge cross section, e.g., $^{56}\text{Fe} \rightarrow \text{Mg}$ from which the individual isotopic cross sections can be inferred. These measurements have generally been at $\sim$600 MeV per nucleon, but for several charges, e.g. ^{56}Fe, ^{32}S, ^{28}Si, and ^{24}Mg, measurements have been made at several energies up to $\sim$1.7 GeV per nucleon. The precision of the measurements ranges from $\sim$3% for cross sections greater than 10 mbarn into neighboring charges (e.g., $\Delta Z < 4$), to $\sim$10% for smaller cross sections where the ΔZ is larger. The second row for each fragment in Table 1 lists the Tsao and Silberberg (1979) cross sections as used previously in the SACLAY propagation program (Engelmann *et al.* 1985). The third row for each fragment in Table 1 gives the percentage contribution to the particular fragment isotope from the indicated beam nucleus. Finally for each secondary isotope we show in column (A) the total percentage contribution to that isotope from all of the primary charges where new cross section measurements are available. These percentages range from $\sim$70% for the production of ^{29}Si and ^{30}Si to 97% for the production of ^{23}Na. Thus overall, using both these direct measurements and the new semi-empirical cross section program of Webber (1987) which has

[1] Space Science Center, University of New Hampshire.
[2] Service d'Astrophysique DPhG/SAP, Centre d'Etudes Nucleares de Saclay.

TABLE 1

MEASURED CROSS SECTIONS AND COMPARISON WITH EARLIER CROSS SECTIONS

FRAGMENT		BEAM ^{23}Na	^{24}Mg	^{25}Mg	^{26}Mg	^{27}Al	^{28}Si	^{32}S	^{40}Ca	^{56}Fe	A	B
	1	36.0	27.5	32.1	29.5	19.0	17.5	13.2	10.9	3.9		
^{21}Ne	2	28.3	24.4	26.5	26.1	17.9	17.0	15.3	6.1	3.2	83%	+7%
	3	6%	27%	8%	7%	4%	22%	4%	2%	3%		
	1	56.8	48.4	28.0	19.3	22.1	21.8	14.9	8.3	2.3		
^{22}Ne	2	57.9	29.8	26.4	24.8	22.6	20.8	15.3	5.8	1.6	94%	+24%
	3	7%	43%	7%	4%	4%	22%	3%	2%	2%		
	1		73.5	47.7	35.5	27.9	24.2	22.6	11.1	2.9		
^{23}Na	2		71.4	28.7	35.4	23.3	21.8	16.1	5.4	2.3	95%	+9%
	3		51%	8%	6%	4%	19%	4%	2%	2%		
	1				76.3	46.5	31.2	24.0	20.7	8.1		
^{25}Mg	2				58.6	31.7	27.1	20.5	15.1	6.1	90%	+17%
	3				21%	11%	39%	7%	5%	7%		
	1					36.0	15.6	9.1	5.9	4.0		
^{26}Mg	2					27.7	16.5	8.6	4.5	3.3	87%	+5%
	3					20%	47%	7%	4%	8%		
	1					35.7	31.9	15.7	8.6	1.9		
^{26}Al	2					31.2	19.4	10.7	5.6	1.6	96%	+30%
	3					14%	67%	8%	4%	3%		
	1						73.9	34.5	17.6	7.1		
^{27}Al	2						68.5	22.2	12.2	5.3	92%	+10%
	3						74%	8%	4%	6%		
	1							40.1	26.1	13.1		
^{29}Si	2							27.4	16.7	10.2	58%	+19%
	3							22%	12%	24%		
	1							45.3	24.8	11.8		
^{30}Si	2							39.1	18.7	10.5	61%	+9%
	3							26%	12%	23%		
	1							69.8	27.8	8.9		
^{31}P	2							60.1	22.3	7.3	80%	+13%
	3							49%	13%	18%		

[1] = New measured UNH cross sections in mbarn.
[2] = Tsao and Silberberg (1979) cross sections in mbarn.
[3] = Percent of fragment produced by beam nucleus.
Col. (A) = Total percent contribution from newly measured cross sections.
Col. (B) = Total percent difference in secondary production using cross sections (1) and (2).

an estimated accuracy of $\pm 10\%$, it is estimated that the interstellar production of all the secondary isotopes listed in Table 1 can be calculated to an accuracy of less than $\sim 5\%$ as compared with $\sim 30\%$ when the earlier semiempirical cross sections of Tsao and Silberberg (1979) were used.

Finally in summary we show in column (B) of Table 1 the total percentage difference in secondary production of a particular isotope that is obtained using the new UNH cross sections as compared with those of Tsao and Silberberg. We note that these differences are all positive and range from a low of $\sim +6\%$ for the production of ^{30}Si to a high of $+28\%$ for the production of ^{26}Al. All of these differences are large enough to have a significant affect on the calculated source abundance of the particular isotope.

For the propagation of cosmic rays we have performed a leaky box calculation with an exponential distribution of path lengths. The program, which is similar to that used by the Saclay group (Engelmann *et al.* 1983, 1985; Soutoul *et al.* 1985) includes nuclear fragmentation and ionization losses. The individual cosmic-ray isotopes are propagated in interstellar hydrogen. The elemental and isotopic source abundances are adjusted to give the best fits to the *HEAO* charge composition data at Earth, and the isotopic measurements of Ne, Mg, Al, and Si at Earth that show the best mass resolution. The input spectra for all species are taken to be power laws in rigidity with exponent $= -2.3$. The escape path length, λ_e, is chosen in conjunction with the solar modulation factor, ϕ, to provide the best fit to the observed B/C ratio using the latest cross sections (Gupta and Webber 1989; Webber and Soutoul 1989). We take $\lambda_e = 24.9\ \beta R^{-0.6}\ g\ cm^{-2}$ for rigidities greater than 4.0 GV and $\lambda_e = 10.8\ \beta$ g cm^{-2} for lower rigidities, along with a solar modulation factor $\phi = 450$ MV. This path length is shown in

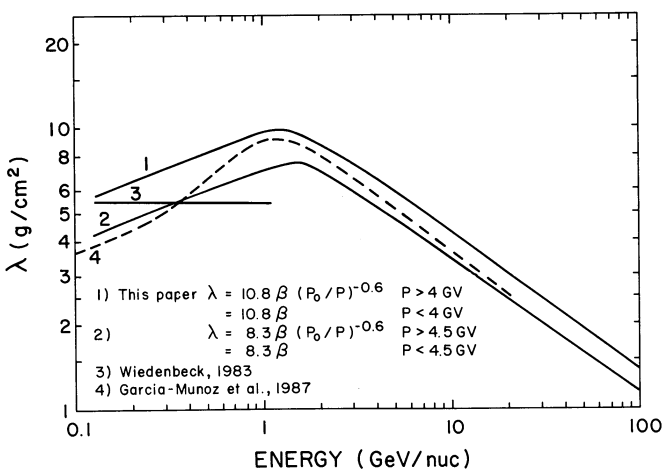

FIG. 1.—Cosmic-ray escape path length as a function of energy

Figure 1, along with other expressions of this path length used previously.

III. THE PROPAGATION OF UNCERTAINTIES AND ESTIMATED OVERALL ERRORS IN SECONDARY PRODUCTION

The abundance ratios of secondary to primary species in cosmic rays at Earth depend on a combination of interstellar path length and the solar modulation, particularly below about 1 GeV per nucleon. The most accurately measured of these ratios is the B/C ratio and this is generally used as a reference for the other ratios. Thus, although the path length dependence and the solar modulation cannot individually be uniquely determined at low energies for each charge ratio, their combination can be determined to the same accuracy with which the B/C ratio is known and can be fitted. In the paper by Webber and Soutoul (1989) which reexamines the $^{13}C/^{12}C$ ratio, it has been estimated that the above escape length fits the spread of available B/C data to an accuracy of less than $\sim \pm 4\%$. The cross sections for boron production should have a similar accuracy to those for the production of the secondary isotopes in the $Z = 9$–16 range. Thus adding these uncertainties in quadrature gives an overall uncertainty in secondary production of less than 6%.

For comparison with previous work using semiempirical cross sections we have not incorporated the fragmentation on interstellar helium in our calculation. Recently Ferrando *et al.* (1988) have reported extensive new measurements of helium-induced cross sections for C, N, O, Al, and Fe nuclei. Their analysis shows that the ratio of helium-induced to hydrogen-induced cross sections is a smooth function of fragment charge, and they utilize this to extrapolate the measured helium cross sections to unmeasured cross sections. Adopting an interstellar helium to hydrogen abundance ratio of 0.10, it is estimated that the resulting change in the production of the nuclei in question is less than 2% relative to B production and is thus neglected in the calculation.

a) Comparison of Predictions and Measurements—Determination of Source Abundances

The predicted abundance ratios of the mainly secondary elements Fl, Na, Al, and P are shown as a function of energy in Figure 2*a*, *b*, *c*, and *d* along with the data from the *HEAO* C-2 experiment at energies greater than 0.8 GeV per nucleon (Engelmann *et al.* 1983). In deriving the predicted curves the source abundances of these elements are adjusted to provide a best fit to the data over the *entire* energy range. For illustration we show in Table 2 the measured abundance at 1 GeV per nucleon and the derived source abundance ratio to Si required to give the best fit to the data, along with the error including both uncertainties on the measurements and on the propagation as described previously. The fit between experimental data and predictions is excellent for all of these secondary elements—generally within a few percent at all energies.

A similar comparison between predictions and measurements for the mostly primary ratios Ne/Si, Mg/Si, and S/Si is shown in Figures 3*a*, *b*, *c*. Here the secondary contribution is generally smaller than the primary contribution at Earth so that the effects of interstellar propagation would be expected to be less. For these ratios the agreement between the predictions and the *HEAO* measurements, while generally good, seems to show systematic deviations as a function of energy. One possible cause for these systematic deviations would be slightly different source spectra for these nuclei. In Table 2 we list the measured abundance ratios at 1 GeV per nucleon along with the derived source abundance ratios obtained in this analysis assuming identical source spectra. In Figures 3*a*, *b*, *c* we illustrate that somewhat better fits to the *HEAO* data are obtained by assuming slightly different source spectra. For Ne the source spectrum is assumed to have a power 0.02 less than Si, for Mg the exponent is 0.02 greater, and for S the spectral exponent is 0.03 less. The significance of these possible spectral differences will be discussed in a later paper.

b) Determination of the Isotopic Composition

We turn our attention now to the isotopic composition of the elements Ne, Mg, Al, and Si and what the new cross section measurements, in conjunction with the currently available data, tell us about the isotopic composition of these elements in the cosmic-ray source. For the selection of data we follow the criteria set forth by Wiedenbeck (1984) in which measurements with significant mass separation, e.g., $\sigma_{mass} < 0.4$ amu, are most heavily weighted. The experiments reporting $\sigma_{mass} < 0.4$ amu for Ne, Mg, Al, and Si isotopes are listed in Table 3 along with other experimental details and the measured mass fractions. Also included in this table is the "best" average mass fraction as derived by Wiedenbeck (1984). These data for Ne, Mg, Al,

TABLE 2

MEASURED AND DEDUCED SOURCE FRACTIONS FOR NUCLEI WITH $Z = 9$–16

Ratio	Measured at GeV per Nucleon	CRS (Si = 1.0)	SEP-SC[a]	LG[b]
Fl/Ne	0.135 ± 0.003	0.000 ± 0.009	0.000 ± 0.0003	0.0008
Na/Mg	0.175 ± 0.005	0.037 ± 0.009	0.067 ± 0.007	0.058
Al/Si	0.235 ± 0.005	0.081 ± 0.006	0.084 ± 0.004	0.085
P/S	0.230 ± 0.010	0.0042 ± 0.0016	0.0049 ± 0.0007	0.0104
Ne/Si	1.08 ± 0.02	0.588 ± 0.024	0.783 ± 0.080	3.30
Mg/Si	1.34 ± 0.02	1.045 ± 0.020	1.089 ± 0.063	1.070
S/Si	0.21 ± 0.01	0.126 ± 0.007	0.242 ± 0.010	0.45
		Agendum		
Ca/Fe	0.226 ± 0.004	0.056 ± 0.005	0.082 ± 0.014	0.063 ± 0.008
Ni/Fe	0.050 ± 0.003	0.054 ± 0.002	0.047 ± 0.008	0.049 ± 0.007
Fe/Si	0.633 ± 0.007	1.032 ± 0.02	1.27 ± 0.16	1.10 ± 0.27

[a] Solar coronal abundances derived from solar energetic particle abundances by Breneman and Stone 1985.

[b] From Meyer 1987.

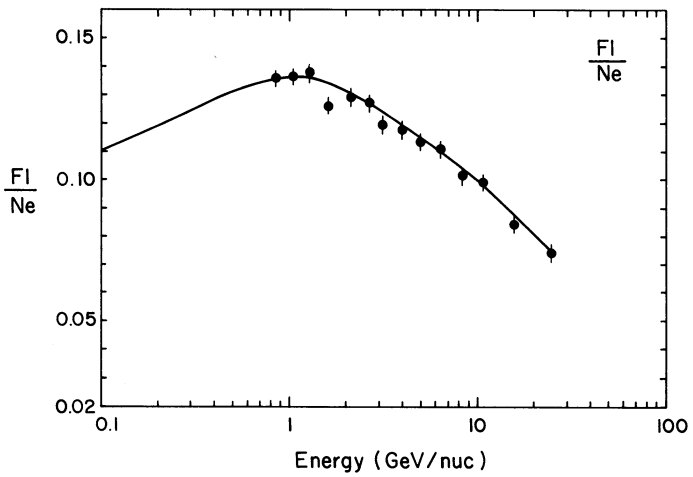

FIG. 2*a*.

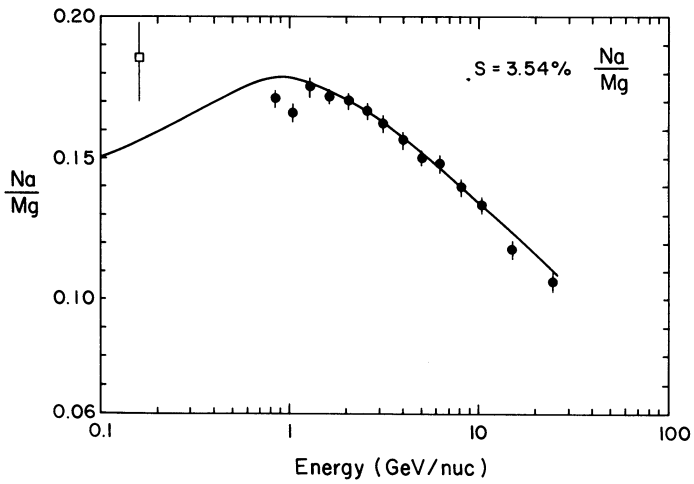

FIG. 2*b*.

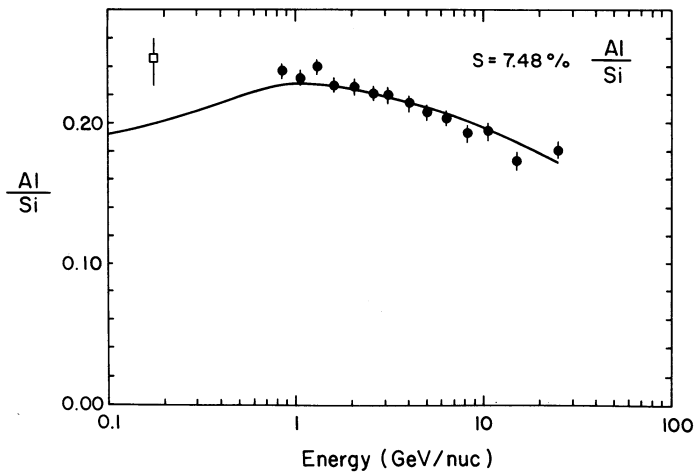

FIG. 2*c*.

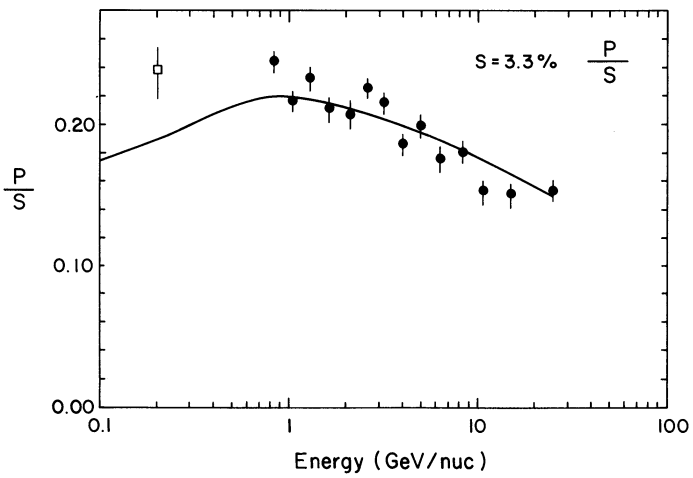

FIG. 2*d*.

FIG. 2.—(*a*) Predicted and observed F1/Ne ratio as a function of energy. Solid circles are *HEAO* C2 data (Engelmann *et al.* 1983); open square is *IMP* data (Garcia Munoz and Simpson 1979). (*b*) Predicted and observed Na/Mg ratio as a function of energy. Symbols the same as Fig. 2*a*. (*c*) Predicted and observed Al/Si ratio as a function of energy. Symbols the same as Fig. 2*a*. (*d*) Predicted and observed P/S ratio as a function of energy. Symbols the same as Fig. 2*a*.

and Si isotopes are plotted in Figures 4, 5, 6, and 7, respectively, along with the predicted isotopic abundances from the propagation program as described earlier, with the source fractions adjusted to give a best fit to the observations (except for ^{21}Ne which is taken to have a zero source abundance). It is seen in Figure 4 that for Ne, the calculated production of ^{22}Ne from this analysis is not greatly different from a typical earlier analyses, defined here as using the Tsao and Silberberg (1979) cross sections and an escape length $\lambda_e = 20.0\ \beta R^{-0.6}$ for $R > 4.0$ GV.

(Note that the percentage change in the calculated source abundance ratio using the full propagation program may differ slightly from the percentage change in the measured cross sections for production listed in Table 1 because of [1] different escape lengths, [2] different source abundances and source fractions, [3] the contribution of unmeasured cross sections.)

For ^{21}Ne, the production calculated using the full propagation program is ~15% higher than a typical earlier calculation at 1 GeV per nucleon; however the prediction is still consistent with a zero source abundance.

For Mg in Figure 5 the calculated production of ^{25}Mg at 1 GeV per nucleon is ~13% higher than earlier calculations, leading to a reduction in the source abundance ratio ^{25}Mg/^{24}Mg by ~0.035. The calculated production of ^{26}Mg at 1 GeV per nucleon is ~8% higher than earlier analyses, leading to a reduction in the source abundance ratio ^{26}Mg/^{24}Mg by ~0.02.

For Al in Figure 6 the calculated production of ^{26}Al at 1 GeV per nucleon is ~30% higher than earlier analyses. This will lead to a considerable reduction in the assumed interstellar density, or conversely an increase in the derived cosmic-ray lifetime using the decay of radioactive ^{26}Al, as discussed in the following section.

For Si in Figure 7 the calculated production of ^{29}Si at 1 GeV per nucleon is ~24% higher than earlier analyses, leading to a reduction in the source abundance ratio to ^{28}Si by ~0.025. The calculated production of ^{30}Si at 1 GeV per nucleon is 17% higher than earlier analyses leading to a reduction in the source abundance ratio to ^{28}Si by ~0.015.

IV. DISCUSSION AND IMPLICATIONS OF NEW SOURCE ABUNDANCES

a) Isotopic Composition

We first discuss the isotopic abundance ratios of Ne, Mg, Al, and Si. The new ratios we derive from our study and the

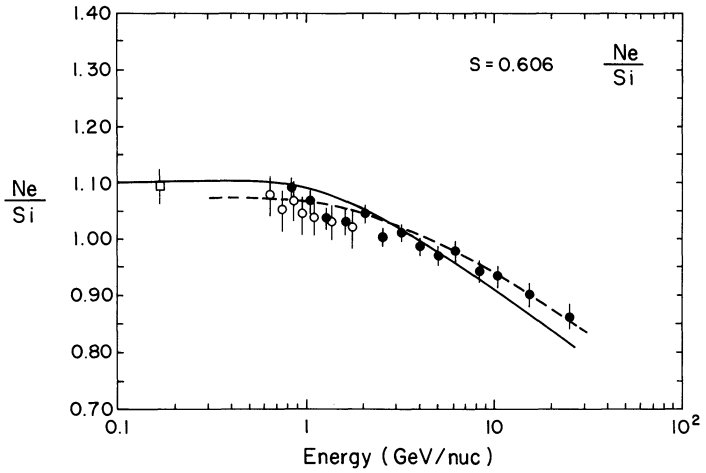

FIG. 3a.

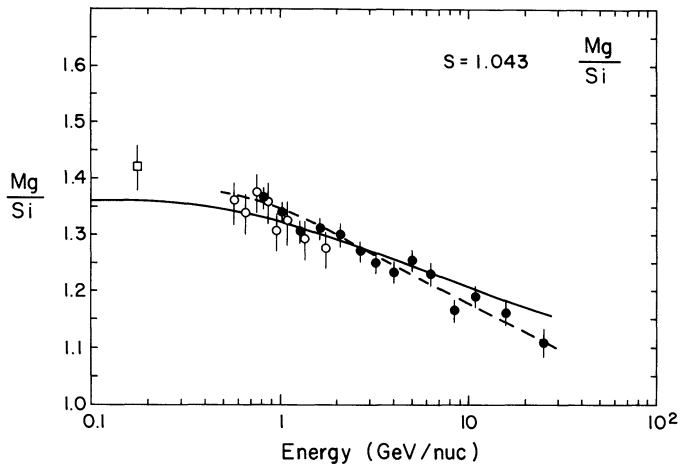

FIG. 3b.

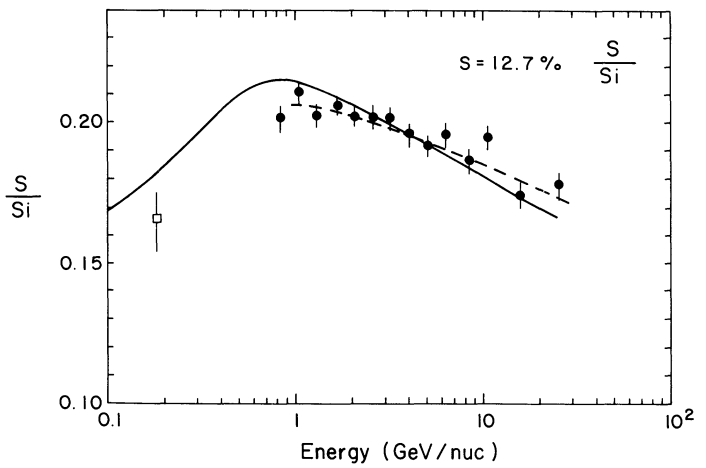

FIG. 3c.

FIG. 3.—(*a*) Predicted and observed Ne/Si ratio as a function of energy. Open circles are balloon data (Webber *et al.* 1985). Other symbols same as Fig. 2*a*. Dashed curve is fit obtained assuming different spectral indices as described in text. (*b*) Predicted and observed Mg/Si ratio as a function of energy. Symbols the same as Fig. 3*a*. (*c*) Predicted and observed S/Si ratio as a function of energy. Symbols the same as Fig. 3*a*.

change in these ratios from earlier values are shown in Table 4 along with the ratios for local Galactic material (essentially the solar photospheric ratios) and the ratios derived for the solar corona based on solar energetic particle (SEP) studies (Mewaldt and Stone 1989). We first compare the cosmic-ray isotopic source (CRS) abundance ratios with the solar photospheric (SP) abundance ratios. This is done in Figure 8, which is adapted from a figure presented by Mewaldt (1987). The ratios originally obtained by Mewaldt are also shown in this figure. For ^{22}Ne the excess we obtain is similar to that given by Mewaldt (1987) and also in other earlier analyses. It is now evident that an excess of ^{29}Si and ^{30}Si in the cosmic-ray source is not indicated by the data. The excess of ^{25}Mg and ^{26}Mg in the cosmic-ray source has been reduced to the 1 σ level when all errors are considered.

In terms of the two possible suggestions to explain the excess of the neutron-rich isotopes, the supermetallicity model of Woosley and Weaver (1981) is clearly less favored by the new source abundances. On the other hand, Wolf-Rayet models (e.g., Casse and Paul 1982) are still consistent with the data, particularly when one considers the revised ^{13}C source abundance derived by Webber and Soutoul (1989). It may be that a more direct comparison for cosmic-ray source abundances is with the composition of a hot environment such as the solar corona, however. Mewaldt and Stone (1989) have recently deduced a new set of solar coronal abundances from solar cosmic-ray measurements which give a similar value for the ^{22}Ne/^{20}Ne ratio but somewhat larger ratios for the Mg isotopes than found in the solar photosphere. In fact, these new solar coronal isotopic ratios for Mg are almost identical to those we deduce for the cosmic-ray source. Thus, although the uncertainties are large, this comparison leads to the conclusion that ^{25}Mg and ^{26}Mg also may not be enhanced in the cosmic-ray source.

Turning now to the radioactive isotope, ^{26}Al, we have already noted that the secondary production of this isotope is greatly increased using the new cross sections. This is shown in Figure 6, where we show the predicted ratio ^{26}Al/Al for an assumed interstellar matter density of 0.3 atoms cm^{-3} using the new cross sections and also using earlier cross sections as calculated by Mewaldt (1987). The data points are the same as given by Mewaldt (1987) and clearly imply now an average matter density less than 0.3 g cm^{-2}. In fact the ^{26}Al data suggest an average matter density 0.18 ± 0.1 atom cm^{-3} slightly less—but still consistent with the estimate of 0.3 atoms cm^{-3} obtained from the other radioactive clock ^{10}Be (Mewaldt 1987) and substantially less than the average density of $\sim$1–2 atoms cm^{-3} measured near the Galactic plane. For an escape pathlength $\sim$7 g cm^{-2} appropriate to the ^{26}Al energy, this leads to a simple lifetime $\sim 4.1 \pm 2.4 \times 10^7$ yr. We note that smaller matter densities have also been derived, using ^{10}Be decay, but with previous cross sections (Simpson and Munoz 1988).

Any difference in the average matter density determined from ^{26}Al decay and ^{10}Be decay may be interpreted in terms of the size of their diffusion region. If, for example, the diffusing region extends several kiloparsecs from the matter disk where the secondary ^{10}Be and ^{26}Al are produced, then because of its shorter decay lifetime, ^{26}Al would be expected to be depressed relative to ^{10}Be (e.g. Owens 1977). In terms of observables this would lead to a smaller matter density (or longer lifetime) as measured by ^{26}Al decay as compared with that measured from ^{10}Be decay. This tendency is apparent in the data when inter-

TABLE 3

MEASUREMENTS OF THE ISOTOPIC COMPOSITION OF Ne, Mg, Al AND Si WITH MASS RESOLUTION, $\sigma < 0.4$ amu

REFERENCE	NUMBER OF EVENTS	σ (amu)	Energy Int meV per nucleon	RATIO TO $n = 0$ ISOTOPE $n = 1$ isotope	$n = 2$ isotope
Neon					
A-1	330	0.20	101–259	0.25 ± 0.05	0.67 ± 0.08
B	31	0.20	30–180	0.11 ± 0.029	0.49 ± 0.10
C-1	548	0.34	423–571	0.14 ± 0.06	0.48 ± 0.05
C-2	211	0.25	407–544	0.19 ± 0.04	0.63 ± 0.09
Avg-Wb (1984)	...	...	300	0.21 ± 0.05	0.58 ± 0.06
Magnesium					
A-1	485	0.22	113–289	0.28 ± 0.035	0.30 ± 0.035
B	57	0.20	30–180	0.31 ± 0.05	0.37 ± 0.08
C-1	773	0.35	471–646	0.22 ± 0.052	0.24 ± 0.024
C-2	407	0.29	426–603	0.27 ± 0.044	0.27 ± 0.028
Avg-Wb (1984)	...	...	320	0.27 ± 0.040	0.27 ± 0.030
Aluminum					
A-3	106	0.23	120–300	0.036 + 0.037 − 0.022	
C-1	144	0.33	481–682	0.048 + 0.058 − 0.037	
C-2	99	0.27	430–627	0.023 + 0.032 − 0.018	
Silicon					
A-2	411	0.24	126–317	0.11 ± 0.02	0.084 ± 0.017
B	30	0.20	30–180	0.070 ± 0.03	0.08 ± 0.03
C-1	531	0.35	496–686	...	0.067 ± 0.028
C-2	285	0.27	446–642	0.070 ± 0.02	0.064 ± 0.018
Avg-Wb (1984)	...	...	340	0.13 ± 0.02 (0.09 ± 0.002)	0.072 ± 0.017

A-1: Wiedenbeck and Greiner 1981*a*.
A-2: Wiedenbeck and Greiner 1981*b*.
A-3: Wiedenbeck 1983.
B: Mewaldt *et al.* 1980.
C-1: Webber 1982.
C-2: Webber *et al.* 1985.

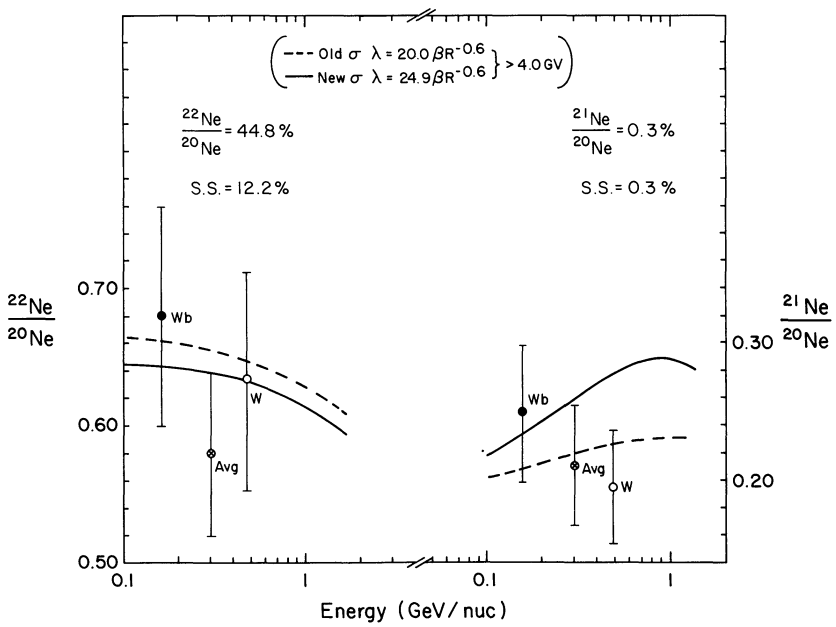

FIG. 4.—Observed and predicted mass fractions for Ne isotopes. Solid circle is data from Wiedenbeck *et al.* (1981*a*, *b*); Open circle from Webber *et al.* (1985); crossed circle is average from compilation by Wiedenbeck (1984) (see also Table 3).

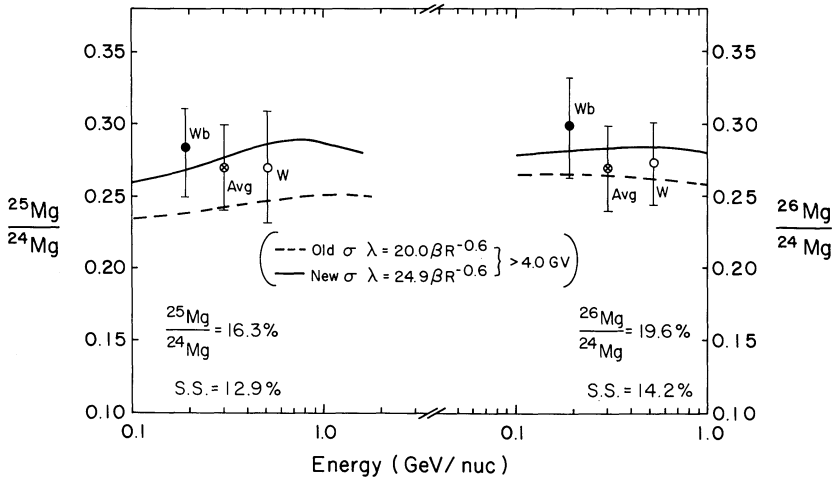

FIG. 5.—Observed and predicted mass fractions for Mg isotopes. Symbols the same as Fig. 4.

preted using the new cross sections; however, the uncertainties in the measurements are still too large for this technique to be used as a useful "measure" of the size of the cosmic-ray diffusing region.

Another example of inhomogeneous matter traversal would be if a significant amount of matter is traversed near the source, early in the cosmic-ray lifetime. In this case the intensity of the long-lived radioactive species ^{10}Be should be greater than the short-lived species, ^{26}Al. This should also lead to the appearance of a shorter lifetime as deduced from ^{10}Be.

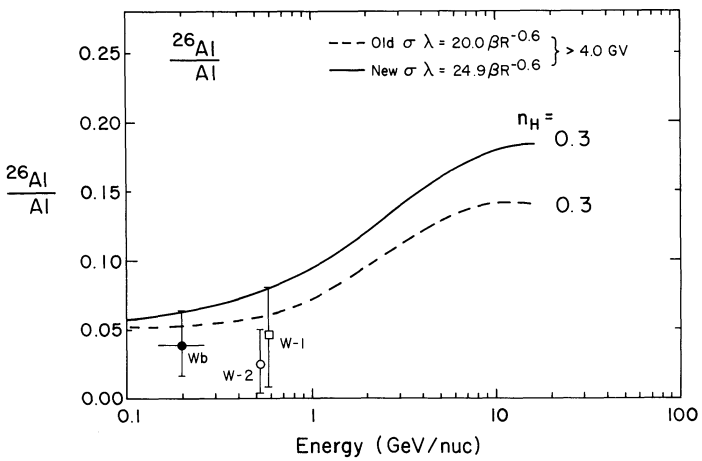

FIG. 6.—Observed and predicted mass fraction for ^{26}Al/Al. Symbols the same as Fig. 4. Solid circle is from Wiedenbeck (1983).

b) Charge Composition

We turn our attention now to the cosmic-ray charge composition at the source. We have already noted that use of the new cross sections changes significantly several of the source abundances of nuclei with $Z = 9$–16. In order to make this study as complete as possible we have redetermined, using the new cross sections, the source abundances of all cosmic-ray nuclei with $Z = 2$–28 again using mainly the measured charge abundance ratios near Earth from *HEAO 3* (Engelmann *et al.* 1983). These additional data are shown as an agendum to Table 2, and also for elements with FIP > 10 eV in Table 5. When the ratios of CRS/LG abundances are formed (see Tables 2 and 5), the well-known decrease for FIP > 9 eV is evident. A similar decrease has been found when the solar

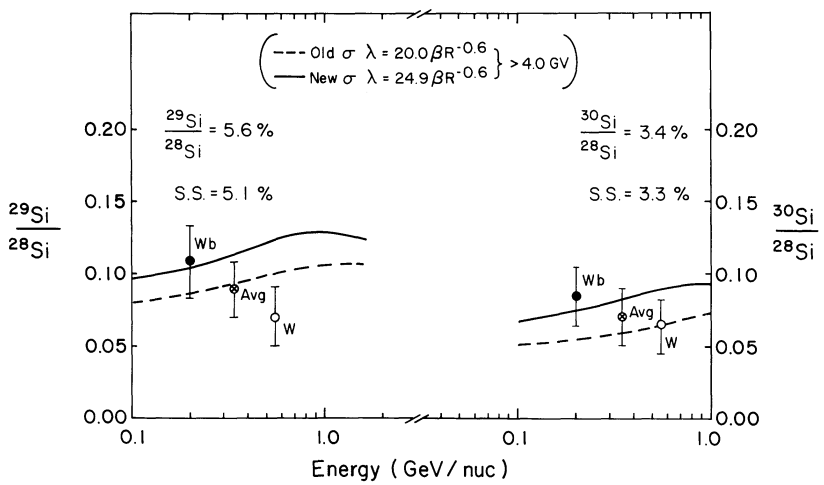

FIG. 7.—Observed and predicted mass fractions for Si isotopes. Symbols the same as Fig. 4.

TABLE 4

SOURCES FRACTIONS FOR Ne, Mg AND Si ISOTOPES

Isotope	CRS	LG = SP[a]	SEP-SC[b]
$^{22}Ne/^{20}Ne$	0.46 ± 0.06	0.122	0.131 ± 0.028
$^{25}Mg/^{24}Mg$	0.16 ± 0.025 (−0.035)[c]	0.129	0.160 ± 0.039
$^{26}Mg/^{24}Mg$	0.195 ± 0.025 (−0.02)	0.142	0.173 ± 0.040
$^{29}Si/^{28}Si$	0.044 ± 0.018 (−0.025)	0.051	
$^{30}Si/^{28}Si$	0.30 ± 0.010 (−0.015)	0.034	

[a] From Cameron 1982.
[b] From Mewaldt and Stone 1989.
[c] Numbers in parenthesis show change in CRS ratios from earlier estimates.

coronal (SC) abundance to solar photospheric (SP) abundance ratio is formed and this has been attributed to fractionization effects related to the fact that low FIP elements may be ionized in the chromosphere whereas high FIP elements may not. For some reason the neutral elements rise from the chromosphere into the corona less efficiently than the ionized elements, thus producing this fractionization (e.g., Breneman and Stone 1985; Meyer 1987). The generally similar effect observed for the SC/SP and CRS/SP ratios has been suggested to imply that a similar fractionization effect may be occurring in the cosmic-ray sources, implying that they too may have selective ionization states in a $\sim 10^4$ K medium. In an attempt to examine whether effects other than the FIP may be influencing the CRS, the data are plotted in a different way in Figure 9, i.e., we plot the ratio SC/SP (which shows the solar FIP effect) versus the ratio CRS/SC (which should emphasize the difference between

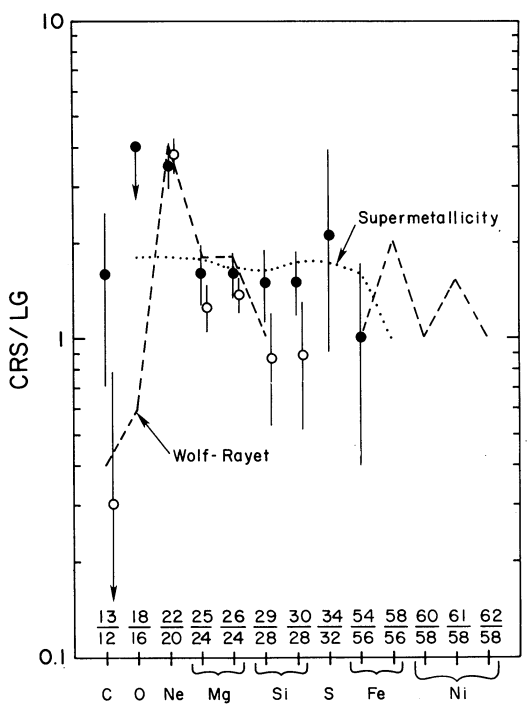

FIG. 8.—Comparison of measured and calculated cosmic-ray source and solar system compositions. Solid circles are data points from the study by Mewaldt (1987); open circles are from this study.

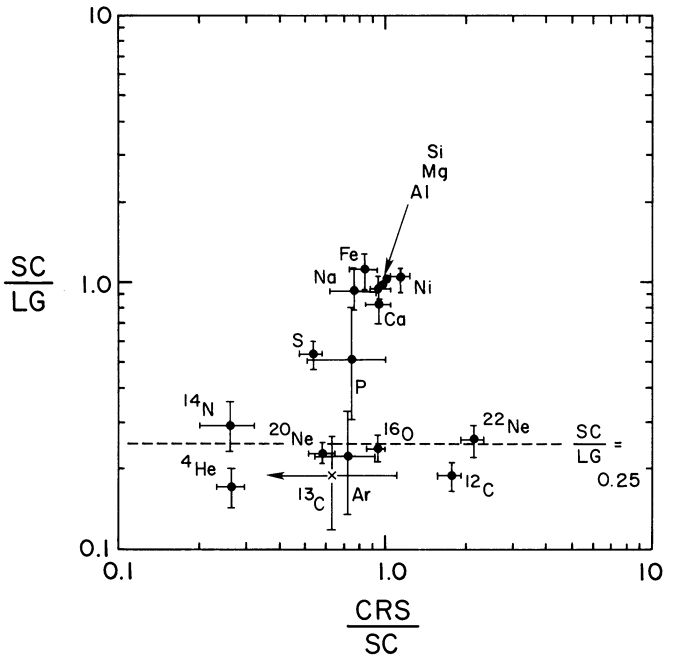

FIG. 9.—Plot of the SC/SP ratio vs. the CRS/SC ratio using CRS data from this paper and SC and SP data as described in Tables 2 and 5.

CRS and SC composition). The dashed line in the figure shows the observed solar coronal/solar photospheric fractionization ratio of 0.25 that has been determined previously to apply for high FIP elements (Breneman and Stone 1985). It is seen that the data clusters in two groups, one consisting of elements with low FIP where SC/SP ≅ 1.0 and one consisting of elements with high FIP where SC/SP ≅ 0.25, with the elements P and S lying in between these two groups. The important point is that *all* of the elements with low FIP also have CRS/SC ≅ one with the possible exception of Na, whereas the elements with high FIP have a broad spread in the CRS/SC ratio. Selective fractionization effects related to FIP, similar to those occurring on the Sun, could also be present in the CRS/SC ratio for high FIP elements; however we suggest that some additional effect is causing the widely different composition relative to the solar corona of *only* the high FIP elements in the cosmic-ray source. In order to identify this effect (or these effects) one needs to look for systematics in the cosmic-ray source abundance of these high FIP elements. One systematic may be the fact that the underabundance of ^{14}N is almost exactly balanced by the overabundance of ^{22}Ne as noted by Gupta and Webber (1989). This could suggest a nucleosynthetic origin for this difference since during the He burning phase in giant stars, ^{14}N is converted into ^{22}Ne and heavier neutron rich isotopes such as ^{26}Mg. Another clue which may point to a nucleosynthetic origin are the ^{12}C and ^{13}C abundances. Webber and Soutoul (1989) have shown that the $^{13}C/^{12}C$ ratio in the cosmic-ray source is less than the solar ratio. Such an effect has been suggested to originate in models in which a fraction $\sim 1/40$ of all cosmic rays are produced by Wolf-Rayet (WR) stars which are rich in ^{12}C so that the ^{12}C abundance is increased by a factor ~ 2, thus reducing the $^{13}C/^{12}C$ ratio (e.g., Prantzos *et al.* 1985). This model also predicts the overabundance of ^{22}Ne that is observed in the CRS. Clearly, the overall picture is probably more involved than we have indicated; the ^{4}He,

TABLE 5

RELATIVE ABUNDANCE OF CHARGES WITH FIP > 10 eV

Charge/FIP	CRS (Si = 1.0)	SEP-SC[a] (Si = 1.0)	LG[b] (Si = 1.0)
S = 10.3 eV	0.126 ± 0.007	0.242 ± 0.010	0.45
P = 10.9 eV	0.0038 ± 0.015	0.0049 ± 0.0007	0.0104
^{12}C = 11.2 eV	4.16 ± 0.08	2.35 ± 0.24	12.6
^{13}C = 11.2 eV	0.016 ± 0.012	0.026 ± 0.010	0.14
Cl = 13.0 eV	<0.007	0.0024 ± 0.0008	0.0052
H = 13.6 eV	...	...	...
O = 13.6 eV	5.22 ± 0.08	5.68 ± 0.35	22.5
N = 14.7 eV	0.182 ± 0.045	0.70 ± 0.05	2.3
Ar = 15.9 eV	0.017 ± 0.005	0.024 ± 0.004	0.107
Fl = 17.3 eV	<0.009	0.0003 ± 0.0003	0.00084
Ne = 21.6 eV	0.588 ± 0.024	0.783 ±	3.30
He = 24.5 eV	121 ± 6	440 ± 30	2700

[a] Solar coronal abundances derived from solar energetic particle abundances by Breneman and Stone 1985.

[b] From Meyer 1987.

^{20}Ne, ^{32}S, and possibly ^{36}Ar abundances appear to be less in the CRS than in the solar corona. These differences as well as the ^{14}N underabundance may suggest a FIP effect in the cosmic ray as well, but an effect that is enhanced by a factor ~3 over that on the Sun. If this is the correct interpretation then ^{12}C and ^{16}O would also be overabundant relative to this enhanced FIP effect. In order to obtain the observed overabundances of these elements would imply that ~1/20 of cosmic rays be accelerated in WR stars.

V. SUMMARY AND CONCLUSIONS

We find that the use of new cross sections in the propagation of cosmic-ray abundances back to their source significantly alters many earlier conclusions regarding the elemental and isotopic composition of nuclei with $Z = 9$–16. In the case of the heavier isotopes of Ne, Mg, and Si, it is found that the data measured at Earth are now consistent with a solar abundance of ^{29}Si and ^{30}Si at the cosmic-ray source. The abundances of ^{25}Mg and ^{26}Mg at the cosmic-ray source are now ~1 σ larger than the solar photospheric abundances and if the solar coronal abundances inferred from SEP by Mewaldt and Stone (1987) are taken as a reference, there is no significant enhancement of ^{25}Mg and ^{26}Mg. The isotope ^{22}Ne remains enhanced in the cosmic-ray source by a factor ~4 over the solar abundance ratio. These new conclusions place new restrictions on the differences between nucleosynthesis in the cosmic-ray source and solar system material. Scenarios which involve a fraction of cosmic rays produced in Wolf-Rayet stars are still viable, although the exact amount of the ^{25}Mg and ^{26}Mg excess is important in this interpretation.

The ^{26}Al measurements now suggest a much smaller interstellar matter density than previously, possibly smaller than that inferred from the longer lived ^{10}Be decay. If this is substantiated by better measurements, this may be used to determine the size of the cosmic-ray diffusing region or the amount of matter traversed early in the cosmic-ray lifetime near the source.

This analysis using the new cross sections allows much better estimates of the source abundances of the elements in the $Z = 9$–16 range. The new source abundance data seem to show that elements with a low FIP have a source composition similar to the solar corona, whereas those elements with a high FIP have a wide spread of compositional differences relative to the corona. Some of these could be nucleosynthetic, e.g., ^{14}N conversion to ^{22}Ne in helium-burning giant stars, and excess production of ^{12}C (and ^{22}Ne) in WR stars. Some of the elemental differences in the CRS could also be due to an enhanced FIP effect in these sources.

This work, including cross section measurements, was supported by NASA grant NGR 30-002-052.

REFERENCES

Breneman, H. H., and Stone, E. C. 1985, *Ap. J. (Letters)*, **299**, L57.
Casse, M., and Paul, J. A. 1982, *Ap. J.*, **258**, 860.
Cameron, A. G. W. 1982, *Essays in Astrophysics*, ed. C. A. Barnes, D. O. Clayton, and D. N. Schramm (Cambridge: Cambridge University Press), p. 23.
Engelmann, J. J., *et al.* 1983, *Proc. 18th Internat.* COSMIC *Ray Conf.*, Bangalore, **2**, 17.
Engelmann, J. J., Goret, P., Julwsson, E., Koch-Miramod, L., Lund, N., Masse, P., Rasmussen, I. R., and Soutoul, A. 1985, *Astr. Ap.*, **148**, 12.
Ferrando, P., *et al.* 1988, *Phys. Rev. C.*, **37**, 1490.
Garcia-Munoz, M., and Simpson, J. A. 1979, *Proc. 16th Internat. COSMIC Ray Conf.*, Kyoto, **1**, 270.
Garcia,-Munoz, M., Simpson, J. A., Guzik, T. G., Wefel, J. P., and Margolia, S. H. 1987, *Ap. J. Suppl.*, **64**, 269.
Gupta, M., and Webber, W. R. 1989, *Ap. J.*, **340**, 1124.
Mewaldt, R. A. 1987, in *Proc. 13th Texas Symposium on Rel. Astrophys.*, World Scientific, Singapore, ed. M. Ulmer, p. 573.
Mewaldt, R. A., Spalding, J. D., Stone, E. C., and Vogt, R. E. 1980, *Ap. J. (Letters)*, **235**, L95.
Mewaldt, R. A., and Stone, E. C. 1989, *Ap. J.*, **337**, 959.
Meyer, J. P. 1987, in *Proc. Symp. Origin and Distribution of Elements* (Singapore: World Scientific), ed. G. J. Mathews, p. 310.
Owens, A. J. 1977, *Ap. Space Sci.*, **40**, 357.
Prantzos, N., Arnould, M., Arcaragi, J. P., and Casse, M. 1985, *Proc. 19th Internat. COSMIC Ray Conf.*, La Jolla, **3**, 167.
Simpson, J. A., and Munoz, M. G., 1988, *Space Sci. Rev.*, **46**, 205.
Soutoul, A., Engelmann, J. J., Ferrando, P., Koch-Miramond, L., Masse, P., and Webber, W. R. 1985, *Proc. 19th Internat. COSMIC Ray Conf.*, La Jolla, **2**, 8.
Tsao, C. H., and Silberberg, R. 1979, *Proc. 16th Internat. COSMIC Ray Conf.*, Kyoto, **2**, 202.
Webber, W. R. 1982, *Ap. J.*, **252**, 386.
———. 1984, in *Workshop on Cosmic Ray and High Energy and Ray Experiments on the Space Station*, ed. by W. V. Jones and J. P. Wefel (Baton Rouge: LSU Press), p. 283.
———. 1987, *Proc. 20th Internat. COSMIC Ray Conf.*, Moscow, **2**, 463.
Webber, W. R., Kish, J. C., and Schrier, D. A. 1985, *Proc. 19th Internat. COSMIC Ray Conf.*, La Jolla, **2**, 88.

Webber, W. R., and Soutoul, A. 1989, *Astr. Ap.*, **215**, 128.
Wiedenbeck, M. E., 1983, *Proc. 18th Internat. COSMIC Ray Conf.*, Bangalore, **2**, 147.
———. 1984, *Adv. Space Res.*, **4**, 15.
Wiedenbeck, M. E., and Greiner, D. E. 1981*a*, *Phys. Rev.*, **46**, 682.
———. 1981*b*, *Ap. J. (Letters)*, **247**, L122.
Woosley, S. E., and Weaver, T. A. 1981, *Ap. J.*, **243**, 561.

M. GUPTA and W. R. WEBBER: Space Science Center, 312 SERB, University of New Hampshire, Durham, NH 03824

P. FERRANDO and A. SOUTOUL: Service d'Astrophysique DPhG/SAP, Centre d'Etudes Nucleares de Saclay, 91191 Gif-sur-Yvette, Cedex, France